J. Fluid Mech. (2004), *vol.* 510, *pp.* 353–373.
DOI: 10.1017/S0022112004009310 Printed in the United Kingdom

Formation of fingers around the edges of a drop hitting a metal plate with high velocity

By NAVID Z. MEHDIZADEH, SANJEEV CHANDRA AND JAVAD MOSTAGHIMI†

Department of Mechanical and Industrial Engineering, University of Toronto, Toronto, Ontario, Canada, M5S 3G8
mostag@mie.utoronto.ca

(Received 13 November 2001 and in revised form 22 January 2004)

Water droplets (0.55 or 1.3 mm diameter) were photographed as they impinged on a stainless steel surface. The droplet impact velocity (10–50 m s^{-1}) and the average roughness (0.03 or 0.23 μm) of the test surfaces were varied. The stainless steel substrate was mounted on the end of a rotating arm, giving linear velocities of up to 50 m s^{-1}. Different stages of droplet impact were photographed by synchronizing the ejection of a single droplet with the position of the rotating arm and triggering of a camera. Finger-shape perturbations were observed around the edges of spreading droplets. The maximum diameter to which a droplet spread and the number of fingers formed around it were measured. The size and number of fingers increased with impact velocity and droplet diameter. At sufficiently high velocities, the tips of these fingers detached, producing satellite droplets. By increasing surface roughness, both the number of fingers and the maximum extent of spreading were decreased. At high impact velocities the spreading liquid film became so thin that it ruptured in several places. A mathematical model, based on linear Rayleigh–Taylor instability theory, was used to predict the wavelength of the fastest growing perturbation around a spreading droplet. The corresponding wavenumber agreed reasonably well with the number of fingers around the droplet.

1. Introduction

Many industrial processes, such as painting, pesticide application, and cooling of hot surfaces, require liquid to be spread evenly over a large area. The easiest way to do this is to spray small droplets (typically 10–1000 μm diameter, depending on the application) at high velocities (10–100 m s^{-1}) onto the surface. High-impact speeds ensure that droplets spread and cover a large area, but they also promote splashing, which is undesirable since it reduces the deposition efficiency (the fraction of sprayed material which adheres to the surface) of the process. Small satellite droplets detach during splashing, bounce off the surface and are swept away by air currents, resulting in both wastage of material and pollution. Experimental studies have attempted to determine conditions under which a droplet will fragment after impact, so that splashing can be avoided in applications. Prediction of such a splashing threshold is complicated by the fact that it depends on not just fluid properties, droplet diameter and impact velocity, but is also a function of surface roughness and wettability.

† Author to whom correspondence should be addressed: mostag@mie.utoronto.ca

A spherical droplet deforms very rapidly after landing on a solid plane, with a thin, circular sheet of liquid jetting out from the initial point of contact between the droplet and surface. The fast advancing liquid–solid contact line is unstable, and a series of regularly spaced waves become visible along it. These perturbations grow larger and form fingers protruding from the periphery of the spreading drop. If the fingers grow sufficiently long, their tips detach, marking the onset of splashing.

Worthington (1876, 1907) was the first investigator to describe in detail the splash of a drop. Using flash illumination from a spark discharge, he took short-exposure photographs of milk and mercury drops as they landed on a glass plate. He noted that the number of fingers formed around the drop increased with both impact speed and droplet diameter. Stow & Hadfield (1981) studied the effects of surface roughness on spreading and splashing of water droplets and established that splashing was promoted by increasing drop diameter (D_d), impact velocity (V_d), and surface roughness (R_a). These droplet impact parameters were combined with liquid density (ρ), viscosity (μ), and surface tension (σ) to give two non-dimensional groupings: the Reynolds number ($Re = \rho V_d D_d/\mu$) and Weber number ($We = \rho V_d^2 D_d/\sigma$). They found that droplets splash only if the so-called 'splash parameter' $K = We^{1/2}Re^{1/4}$ exceeds a critical value (K_c), which depends on the surface roughness. Cossali, Coghe & Marengo (1997) combined the data from this study with those of Mundo, Sommerfeld & Tropea (1995) and Yarin & Weiss (1995), to develop an empirical correlation between K_c and R_a. Range & Feuillebois (1998) found that the onset of splashing was relatively insensitive to fluid viscosity, and that splashing occurred if We was greater than a critical number, whose magnitude was a function of surface roughness.

What mechanism triggers the growth of fingers around the periphery of an impacting drop? There is some debate in the literature regarding the nature of the instability responsible (Rein 1995). Allen (1975) offered the hypothesis that fingering is initiated by Rayleigh–Taylor instability generated at the interface between two fluids of different density when the lighter fluid pushes the heavier one (Sharp 1984). Fingers, according to this theory, form immediately upon impact and then grow larger as the drop spreads. Alternatively, Rein (1995) speculated that fingers are created during droplet spreading as liquid flows over the solid surface, though he did not prescribe any detailed mechanism.

Experimental evidence seems to support the view that fluid instability during the first instant of impact determines the number of fingers formed. Thoroddsen & Sakakibara (1998) photographed water droplets from below as they landed on a glass plate, and found that fingers are visible even in the earliest stages of impact. Loehr (1990) used multiple-exposure photographs of spreading droplets to show that the number of fingers remained constant. Aziz & Chandra (2000) photographed molten tin droplets splashing on a hot steel plate, and also noted that the number of fingers changes very little during the outward spreading of the droplet.

As a droplet spreads over a solid surface that has microscopic protrusions on it, the liquid velocity is perturbed over a wide range of frequencies. The spacing between fingers corresponds to the wavelength of the fastest growing instability. If we neglect the curvature of the droplet surface and assume the liquid–air interface to be planar, linear Rayleigh–Taylor instability analysis predicts that the fastest growing disturbances will have a wavelength (Chandrasekhar 1961; Allen 1975):

$$\lambda = 2\pi\sqrt{\frac{3\sigma}{a\rho}}, \tag{1.1}$$

where a is the deceleration of the interface. Allen (1975) estimated $a = V_d^2/(D_{max}/2)$, with D_{max} the diameter of the droplet at its maximum extension, so that the number of fingers $N = \pi D_{max}/\lambda$. He counted the number of fingers around ink blots formed by drops falling on a piece of paper, and demonstrated reasonable agreement between experiments and predictions. Loehr & Lasek (1990) criticized Allen's assumption of constant deceleration and suggested that a more detailed analysis of spreading dynamics was required. Marmanis & Thoroddsen (1996) obtained blots from a number of liquids falling on sheets of paper, and correlated the number of fingers as $N \sim (We^{1/4}Re^{1/2})^{3/4}$.

Bhola & Chandra (1999) took a slightly different approach to the model of Allen (1975) proposing that $a = V_d^2/(D_d)$, and using a simple energy balance model to calculate D_{max}, obtained:

$$N = \frac{We^{0.5}Re^{0.25}}{4\sqrt{3}} = \frac{K}{4\sqrt{3}}. \tag{1.2}$$

This analysis gave a theoretical basis for the splash parameter, K, which had previously been established empirically.

Kim, Feng & Chun (2000) presented a much more sophisticated instability analysis of the liquid sheet emerging from under an impacting drop, solving the potential flow equation. They neglected the effect of viscosity, arguing that fingers are initiated immediately after droplet impact when viscous forces are small, and solved the governing equations numerically to obtain the fastest growing wavelength as a function of *We*. Since viscous effects were disregarded, the solution was independent of *Re*. There is experimental evidence to justify omitting viscosity. Though Loehr (1990) had proposed a linear variation of the number of fingers with *Re*, Range & Feuillebois (1998) showed they could not correlate their experimental data for fingers around droplets of water–glycerine and water–ink mixtures in this way. The number of fingers was sensitive to the surface tension of a liquid, not its viscosity.

Bussmann, Chandra & Mostaghimi (2000) simulated droplet splashing using a three-dimensional numerical model of fluid flow. The model successfully simulated the growth and detachment of fingers. Instability to trigger growth of fingers was introduced artificially in the model by imposing a sinusoidal perturbation on fluid velocity immediately after droplet impact. The number of fingers formed was therefore an input to the model, rather than being predicted by it.

Bussmann, Chandra & Mostaghimi (2000) collected published data on the number of fingers around impacting droplets of water, hydrocarbons, liquid metals and molten salts and found that (1.2) gave predictions that agreed reasonably with experiments. However, the range of available data was quite limited, all of it being obtained from a few experiments that were quite similar to each other: droplets, 1–5 mm in diameter, were dropped onto a solid surface, reaching impact velocities of at most $9\,\mathrm{m\,s^{-1}}$, with *We* usually less than 10^3. Some data for high impact velocities can be obtained from thermal spray processes, where molten droplets are propelled onto a surface by a high-temperature jet, landing with typical values of $We \sim 10^4$ and $Re \sim 10^3$ (Bussmann *et al.* 1998). Equation (1.2) predicts $N \sim 80$; comparison with micrographs of splats formed by solidification of molten alumina droplets in a plasma spray after impact on a steel plate shows this to be an overestimation (Bussmann *et al.* 1998). Obviously, the simple approximations made to derive this equation are not valid at high Weber number.

While a number of investigators (Allen 1975; Bhola & Chandra 1999; Kim *et al.* 2000; Bussmann *et al.* 2000) have surmised that Rayleigh–Taylor instability causes

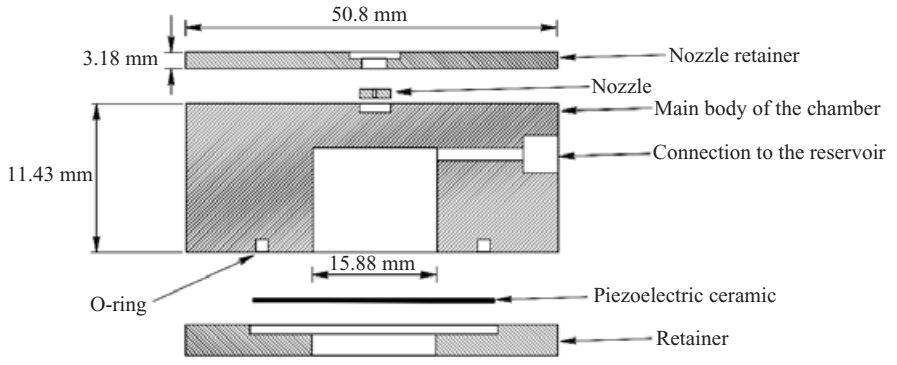

FIGURE 1. Diagram of the cross-section of the nano-litre water droplet generator.

fingering around the edges of an impacting droplet, this hypothesis has not been conclusively demonstrated by comparison with experiments. We proposed a simple test: can Rayleigh–Taylor instability theory predict the number of fingers formed around splashing drops over a wide range of impact velocities?

The objective of our study was to photograph splashing of water droplets impinging on a steel plate with high Weber number ($\sim 10^3 - 10^5$), almost two orders of magnitude larger than those previously reported in the literature, and representative of droplet impact conditions in many industrial applications. For a given liquid, *We* can be raised by increasing either the droplet diameter or impact velocity. In practice, water droplets with diameters larger than about 2 mm become non-spherical, making analysis difficult. We chose to keep the droplets small (with diameters of either 0.55 mm or 1.3 mm), ensuring that they remained spherical, and varied impact velocity from 10 to 50 m s^{-1}. Droplet impact and splashing was photographed on two different stainless steel surfaces with average roughness of either 0.03 or 0.23 μm. From these images, we counted the number of fingers that form around the periphery of a drop as it splashes.

We used linear Rayleigh–Taylor instability theory to calculate the number of fingers forming around an impacting drop as a function of *We*. We solved the governing equations analytically (rather than numerically, as Kim *et al.* 2000 did) and demonstrated that predictions from the model agreed well with our measurements.

2. Experimental apparatus and procedure

2.1. *Water droplet generator*

We produced uniform sized water droplets with a piezoelectric droplet generator, built using a design described by Yang *et al.* (1997). Figure 1 shows the droplet generator body, which was made of stainless steel. A piezoelectric ceramic disk (American Piezo Ceramics, Model APC352428A) formed one wall of the chamber, which was filled with water. A retainer ring held the disk firmly against the droplet generator body, which was sealed with a silicone o-ring. A commercially available synthetic sapphire nozzle (Swiss Jewel Company, Philadelphia, PA) was inserted into a hole drilled through the other wall of the chamber and sealed in place with epoxy adhesive. The droplet generator was operated with the nozzle pointing downwards. The chamber was connected with plastic tubing to a reservoir filled with deionized distilled water. The system was primed by raising the reservoir above the chamber until water jetted out through the nozzle. After making sure that no bubbles were trapped inside the

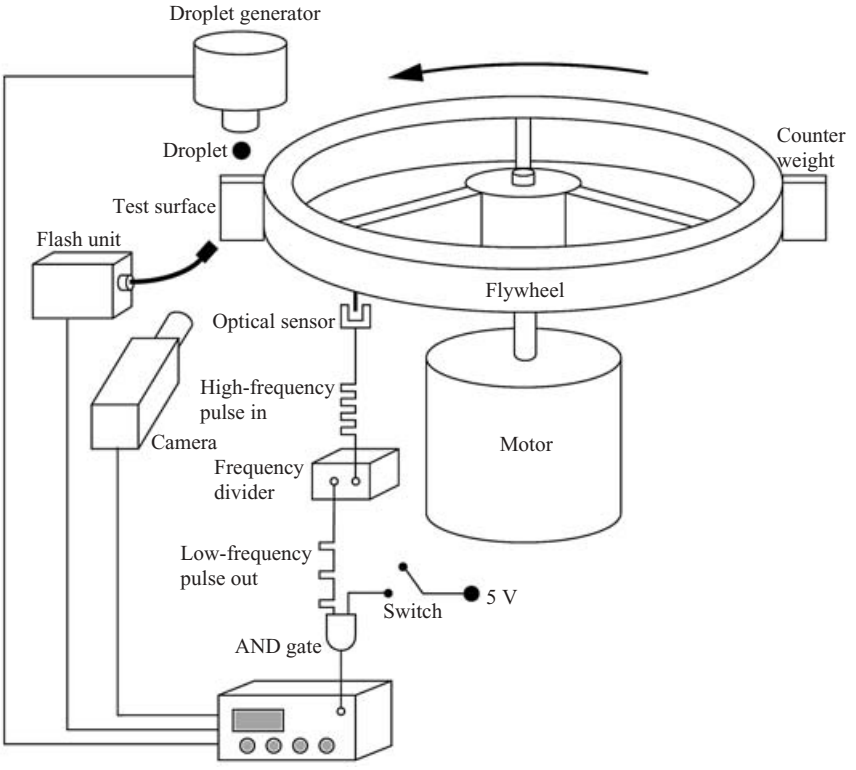

FIGURE 2. Diagram of the experimental apparatus.

chamber, the reservoir was lowered, reducing the hydrostatic head above the chamber just enough to prevent any water from emerging through the nozzle. Applying a voltage pulse across the piezoelectric disk made it flex and forced water out through the nozzle, producing a droplet. The droplet generator was driven with square wave pulses of 40–100 V amplitude and 10–50 ms duration at frequencies as high as 5 Hz. The uncertainty of diameter measurement was $\pm 40\,\mu$m in our experiments.

2.2. *High-speed impact apparatus*

To achieve high-impact velocities, it is easier to accelerate the substrate rather than the droplet. One way of doing this is to mount the substrate on the end of a rotating arm. Figure 2 shows a diagram of the apparatus we built to capture images of droplet impact by synchronizing the ejection of a droplet from the generator with the position of the moving substrate.

The test surface was a stainless steel plate ($10 \times 10\,\text{mm}^2$; 6.3 mm thick) bolted to one end of a 300 mm long, 6.35 mm diameter stainless steel shaft; an identical plate was fixed at the other end of the shaft to act as a counterbalance. The centre of the shaft was mounted on the hub of a variable speed d.c. motor (Model CYMM-82700-51, Electromate, Woodbridge, ON) (see figure 2). By varying the voltage applied to the motor, rotational speeds of up to 3500 r.p.m. were obtained, giving the test surface linear velocities of up to $55\,\text{m}\,\text{s}^{-1}$. The velocity of the droplet as it fell to the test surface's plane of rotation was less than $1\,\text{m}\,\text{s}^{-1}$, which was small enough to assume that impact was normal to the surface even for the lowest velocities in our experiments, $10\,\text{m}\,\text{s}^{-1}$.

Two different test surfaces were used. One was polished on a metallurgical wheel to a mirror finish and its average surface roughness (R_a) was measured using a surfometer (series 400, Precision Devices, Milan, Michigan) to be 0.03 μm. The other surface was first sand-blasted and then polished with emery paper to give $R_a = 0.23$ μm.

At the highest velocities, the approach of the rotating arm produced a small but measurable deformation in droplets prior to impact, making them slightly elliptical in shape. In such cases, we measured the major (a) and minor (b) axes of the ellipse, and defined an equivalent diameter $D_{eq} = (ab)^{1/2}$, which was used in all subsequent calculations. The difference between D_{eq}, a and b was always less than 3%.

Because the substrate was rotating about a fixed point, two additional forces – centrifugal and Coriolis – were imposed upon an impacting droplet, which appear as additional body forces in the Navier–Stokes equations. An order-of-magnitude analysis of the Navier–Stokes equations showed that for $D_d/R_f \ll 1$ (where R_f is the distance between the centre of the droplet and centre of rotation), which was the case in our experiments, both centrifugal and Coriolis forces may be neglected.

2.3. *Photographing droplet impact*

A CCD video camera (Sensicam, Optikon Corporation, Kitchener, ON) equipped with a 90 mm macro lens was used to photograph droplet dynamics during impact. It had an intensified CCD chip capable of recording 30 frames per second with a resolution of 1280 × 1024 pixels. The camera could also superimpose up to ten images in every frame, each with an exposure time as short as 0.1 μs, separated by delays that varied from 0 to 1 ms (selectable in 0.1 μs time steps). A 0.1 μs exposure time was short enough to capture the deformation of the droplet during the impact, without any blurring caused by the extremely fast motion of the substrate.

To hit a falling droplet with the moving substrate, and to photograph its impact, three events had to be synchronized with the position of the arm: ejecting a droplet, triggering the camera, and setting off a flash to provide illumination. An optical sensor (Model HOAO880, Honeywell Optical Switch, Toronto, ON) was used to detect the instant the rotating arm passed over it. This signal was then used to trigger the camera, flash and droplet generator. Since the frequency of the optical sensor signal was too high to directly drive the droplet generator, it first passed through a frequency divider, reducing it by a factor that varied from 2 to 32, depending on the rotational speed of the arm. The low-frequency signal formed one input of an AND gate (see figure 2).

When we were ready to take a photograph, we pressed a switch which activated the second input of the AND gate, so that the pulses at the other input were transmitted to a time delay unit. The rising edge of each pulse provided a reference that was used to time all other events. The digital time-delay generator (Model DG 535, Stanford Research Systems, Sunnyvale, CA) controlled the timing of three subsequent actions with pico-second resolution. We made droplets collide with the substrate by adjusting the delay between the reference signal and the triggering of the droplet generator. Each droplet produced by the generator fell to a position coincident with the centre of the test surface just as the arm approached the droplet. The flash (Model MVS 7000, EG&G, Salem, MA) timing was adjusted so that droplet impact was illuminated by a 10 μs long burst of light. While the flash was on, the camera was activated to take a single 0.1 μs exposure of an impacting droplet. By varying the time at which the camera was triggered, different stages of droplet impact were recorded, and the entire process of droplet impact was reconstructed from a sequence of such pictures.

This single-shot method of photography provided much higher resolution pictures than could be obtained from a high-speed video camera, which allowed us to observe very small satellite drops. Its chief disadvantage was that there was significant uncertainty (approximately $\pm 20\,\mu s$) in identifying the time from impact of each image owing to variations in droplet generation time. Since this was about the same as the interval between frames in a photographic sequence, we were unable to accurately assign a time to each picture. However, this did not prove a serious shortcoming, since our main objective was to count the number of fingers around a droplet when it had spread to its maximum diameter. By taking multiple images of a spreading droplet in the same frame we could easily identify maximum spread diameter.

Digital images from the camera were transferred to a computer for analysis and dimensions of the impacting drop were measured using image analysis software (IMAGE, National Institute of Health, Bethesda, MD). The resolution of these measurements, corresponding to one pixel of the digital image viewed on a computer monitor, was $5\,\mu m$.

3. Results and discussion

3.1. *Water droplet impact photographs*

Figure 3 shows different instants during the impact, spreading and recoil of 0.55 mm diameter water droplets landing with a velocity of $10\,m\,s^{-1}$ on a stainless steel surface with $R_a = 0.03\,\mu m$. The droplets were photographed from above with the camera aligned along the direction of motion of the test surface. The images in figure 3 are labelled *a* to *h*, indicating successive stages of spreading. Droplets spread to their maximum diameter (figure 3*f*) in about $150\,\mu s$, and were then pulled back by surface tension. The periphery of the droplets remained quite smooth during impact, with very small perturbations visible as they spread. In this case, fingers initiated around the droplets did not grow larger, but were damped out (figure 3*h*).

Figure 4 shows the impact of droplets with the same diameter and velocity as those in figure 3, but on a much rougher surface ($R_a = 0.23\,\mu m$). The image quality is not as good as before, because of poor light reflection off the surface. However, it can clearly be observed that the effect of increasing surface roughness was to magnify the amplitude of perturbations around the droplet edge, producing distinct fingers (figure 4*f*). These fingers later merged and disappeared as droplets recoiled, forming a ring around their rims (figure 4*h*).

Figure 5 shows the impact of water droplets with a velocity of $20\,m\,s^{-1}$ on a stainless steel surface with $R_a = 0.03\,\mu m$. The time to spread to the maximum diameter (figure 5*f*) was about $70\,\mu s$. Both the number of fingers observed around the circumference of the droplets and their maximum spread diameter increased with impact velocity. The fingers were evenly spaced around the droplet periphery, and prominent enough to be counted clearly (figure 5*d*). A few of the fingers became large enough to detach, producing satellite droplets (figure 5*e*). A similar experiment was performed on a rough surface ($R_a = 0.23\,\mu m$) and it was observed that the number of fingers decreased as surface roughness increased, although individual fingers were larger. Also, on the rough surface, droplets retracted less after spreading than they did on the smooth surface.

Figure 6 is a sequence of photographs of droplets impacting with a velocity of $40\,m\,s^{-1}$. Long, narrow fingers are visible around the droplets immediately after impact. These fingers detached, producing a large number of satellite droplets. The liquid film produced by a spreading droplet became so thin that it ruptured at several

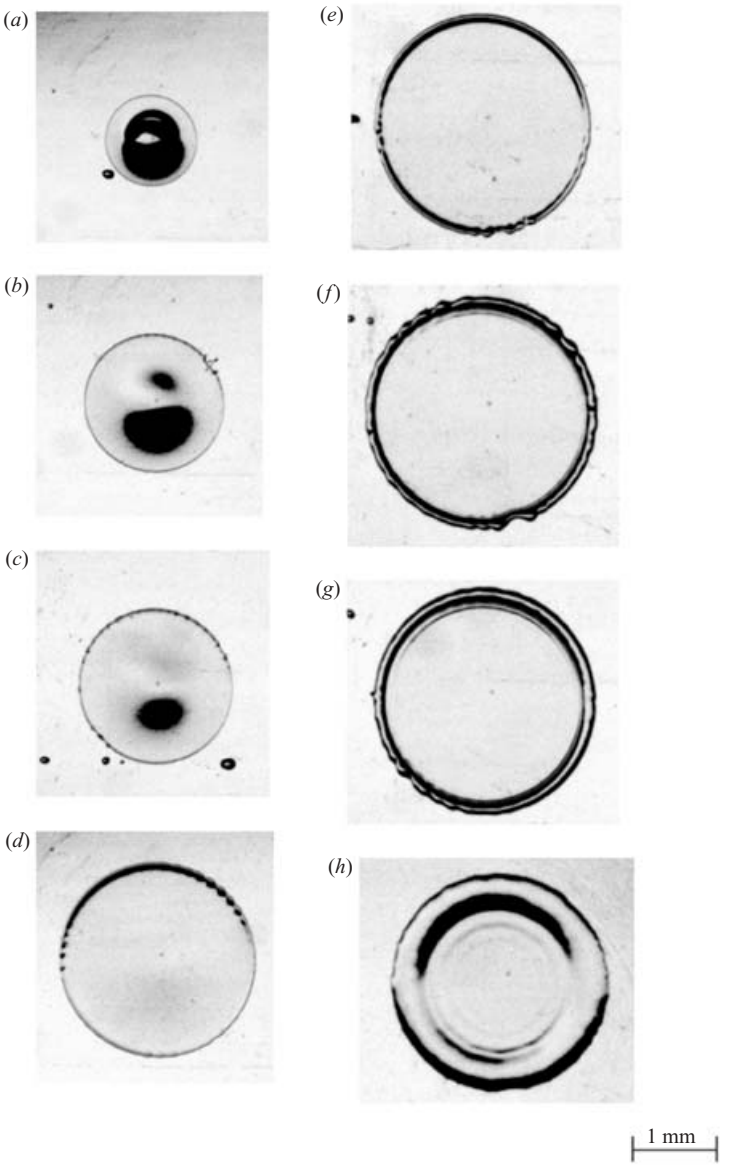

FIGURE 3. The impact of a 0.55 mm water droplet on a stainless steel surface with the impact velocity of 10 m s^{-1}. The time to spread to the maximum diameter is 150 μs ($R_a = 0.03$ μm, $Re = 5500$, $We = 753$).

points, forming dry patches (figures 6*g* and 6*h*). The liquid ring around the edge of the droplet is not symmetric in the last frame (figure 6*h*), because centrifugal forces produced by the rotation of the substrate become important at high angular velocities.

Figure 7 shows 0.55 mm diameter droplets at their maximum spread for five different impact velocities, ranging from 10 to 40 m s^{-1}. Close examination of the photographs showed that in all cases a small bubble formed at the centre of the droplet immediately after impact. The bubble has previously been observed by Chandra & Avedisian

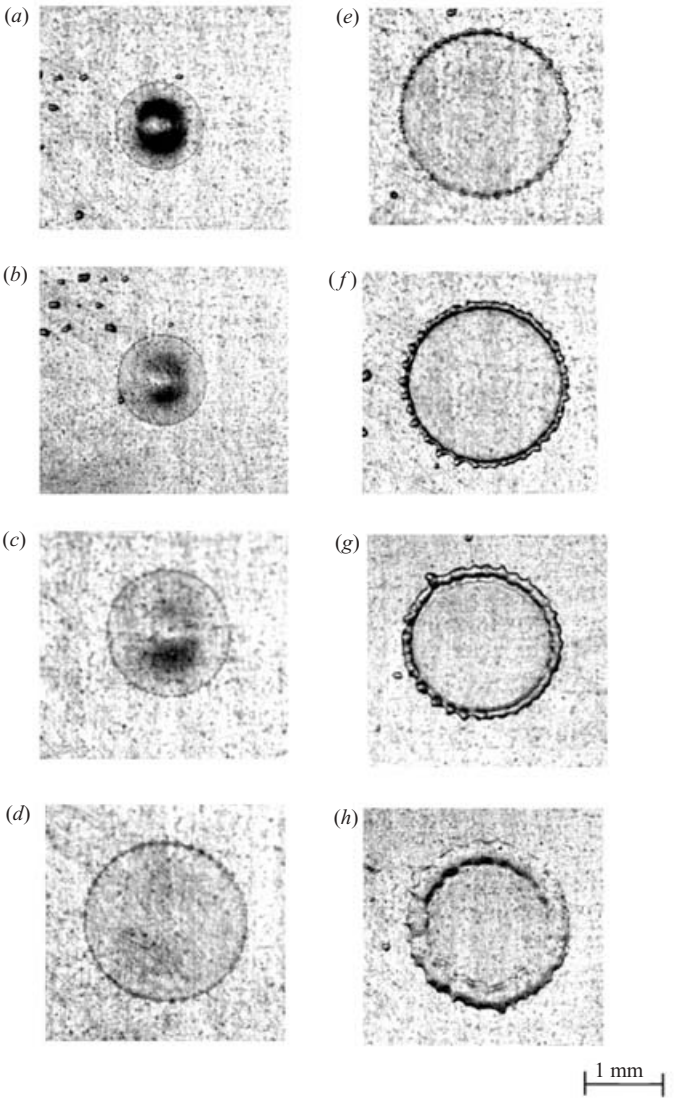

FIGURE 4. The impact of a 0.55 mm water droplet on a stainless steel surface with an impact velocity of 10 m s^{-1}. ($R_a = 0.23$ μm, $Re = 5500$, $We = 753$).

(1991), who attributed it to air being trapped at the point of impact of the droplet. The size and number of fingers increased with impact velocity, as is clearly evident in the photographs. From these, and other similar images, we measured both the maximum spread diameter of the droplets and the number of fingers. We recorded these quantities for ten different droplets under the same impact conditions and averaged the results. In some of the low impact velocity cases there were sections of the droplet periphery where fingers were too small to be seen clearly (for example, see figure 7*b*). In such cases, we counted fingers on the half of the droplet where they were distinct and doubled that number to obtain N. Droplet diameters were measured from the base of the fingers. At the highest impact velocities, the spreading liquid film was rather irregular (figure 7*e*) producing greater scatter in the data. In all cases, N varied by, at most, $\pm 10\%$ of the mean value.

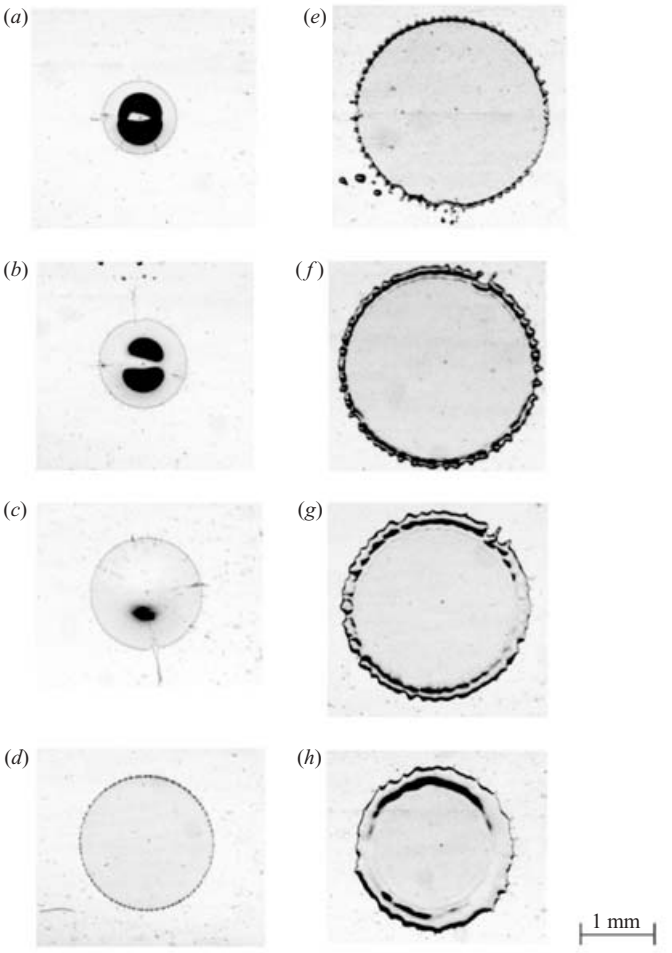

FIGURE 5. The impact of a 0.55 mm water droplet on a stainless steel surface with an impact velocity of 20 m s^{-1}. The time to spread to the maximum diameter is 70 μs ($R_a = 0.03$ μm, $Re = 11\,000$, $We = 3014$).

Table 1 gives the different combinations of droplet diameter impact velocity and surface roughness for which we photographed droplet impact, the number of fingers and the impact conditions in our tests. The calculated values of *We* and *Re* are given in each case, and the average number of fingers counted. It can be seen that the number of fingers increased with impact velocity, and that there were fewer fingers formed when a droplet landed on the rough surface compared to the smooth surface.

Previous workers (e.g. Stow & Hadfield 1981; Mundo *et al.* 1995; Cossali *et al.* 1997) have attempted to define a 'splashing threshold', defined as the lowest impact velocity at which satellite droplets are visible. However, specification of such a threshold is rather arbitrary. For example, it was difficult to decide by examining photographs whether splashing occurred at an impact velocity of 20 m s^{-1} (figure 5), when only a few satellite droplets were evident. Sometimes small droplets were visible immediately after impact, but not later when the droplet was at its maximum extent. Figure 8(*a*) shows a 0.55 mm droplet shortly after impacting with a velocity of 30 m s^{-1}. Very

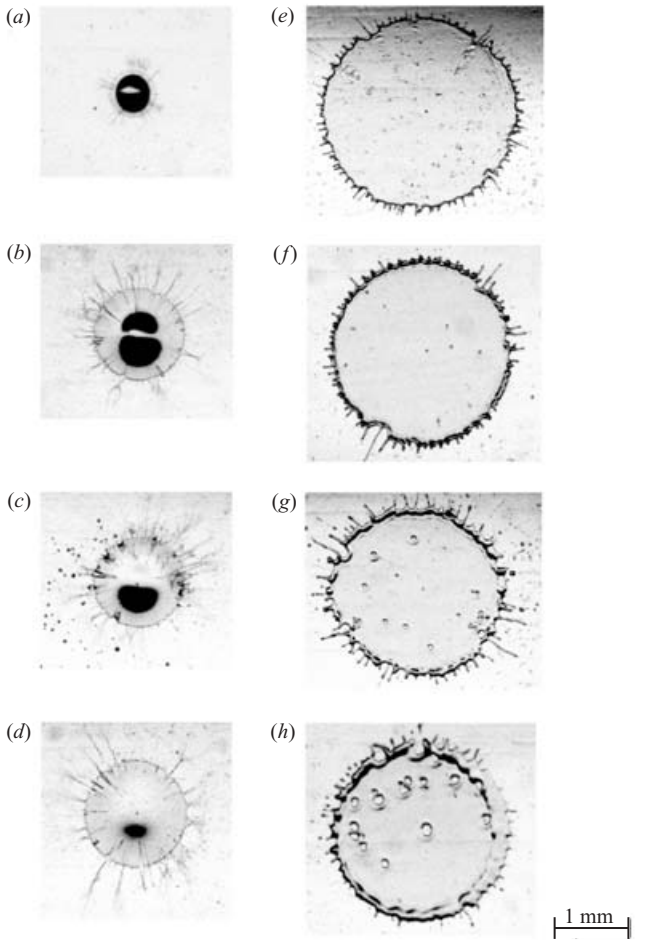

FIGURE 6. The impact of a 0.55 mm water droplet on a stainless steel surface with an impact velocity of $40\,\mathrm{m\,s^{-1}}$. The time to spread to the maximum diameter is 40 μs ($R_a = 0.03$ μm, $Re = 22\,000$, $We = 12\,055$).

small satellite droplets are seen around the droplet, but these were not evident in later frames. At impact velocities above $40\,\mathrm{m\,s^{-1}}$, entire sheets of liquid, rather than single drops, detached after impact (figure 8*b*). Given these uncertainties, we did not attempt to define a splashing threshold.

3.2. *Maximum spread factor*

We measured the maximum extent that droplets spread at each velocity. The maximum spread diameter (D_{max}) was non-dimensionalized by the initial droplet diameter (D_d) to give a 'maximum spread factor' ($\xi_{max} = D_{max}/D_d$). Figure 9 shows the variation of ξ_{max} with Reynolds number ($Re = \rho V_d D_d/\mu$) for impact on two surfaces with average roughness (R_a) of 0.03 μm and 0.23 μm, respectively. Each symbol marks the average value measured for five different droplets. Error bars mark the maximum and minimum values recorded. The error was largest at high velocities, where splashing made the droplet shape irregular (see figure 7*e*). Droplet spreading was slightly reduced by increasing surface roughness.

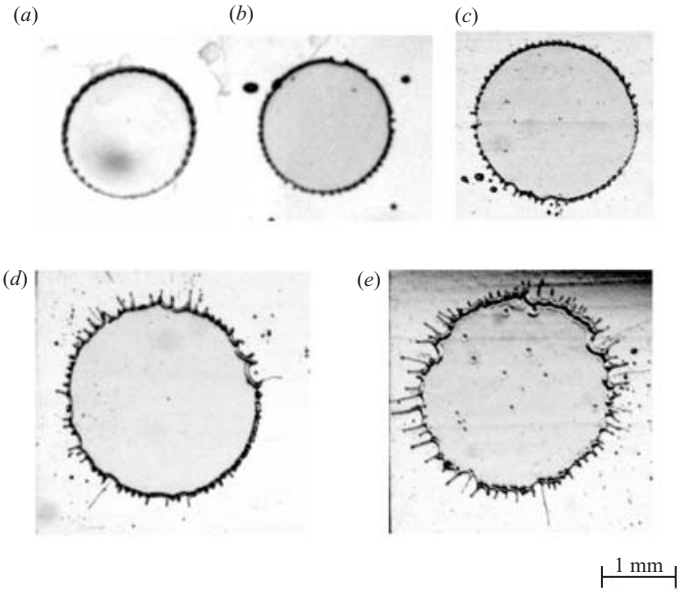

FIGURE 7. Shape of a 0.55 mm water droplet impinging on a stainless steel surface ($R_a =$ 0.03 μm) at its maximum spreading: (*a*) $V_0 = 10\,\mathrm{m\,s^{-1}}$; $N = 36$; (*b*) 15, 55; (*c*) 20, 61; (*d*) 30, 79; (*e*) 40, 84.

D_d(mm)	V_d(m s^{-1})	*Re*	*We*	N_{exp}	N_{pred}	R_a(μm)
0.55	10	5500	753	36	31	0.03
0.55	15	8250	1694	55	47	0.03
0.55	20	11 000	3014	67	62	0.03
0.55	30	16 500	6781	79	91	0.03
0.55	40	22 000	12 055	84	124	0.03
0.55	10	5500	753	46	31	0.23
0.55	15	8250	1694	52	47	0.23
0.55	20	11 000	3014	61	62	0.23
0.55	30	16 500	6781	68	91	0.23
0.55	40	22 000	12 055	80	124	0.23
1.30	20	26 000	7123	132	96	0.03
1.30	36	46 800	23 079	148	170	0.03
1.30	40	52 000	28 493	142	190	0.03
1.30	45	58 500	36 061	150	211	0.03
1.30	50	65 000	44 520	158	235	0.03

TABLE 1. Comparison of measured (N_{exp}) and predicted (N_{pred}) numbers of fingers around droplets at their maximum extension.

Estimates of the extent of droplet spreading have previously been developed (Chandra & Avedisian 1991; Pasandideh-Fard *et al.* 1996) based on simple energy conservation models of droplet impact. These models calculate the initial droplet kinetic energy and surface energy prior to impact, and equate it to the final surface energy at the instant when the droplet has spread to its maximum diameter and is stationary, plus the energy dissipated in overcoming liquid viscosity that resists

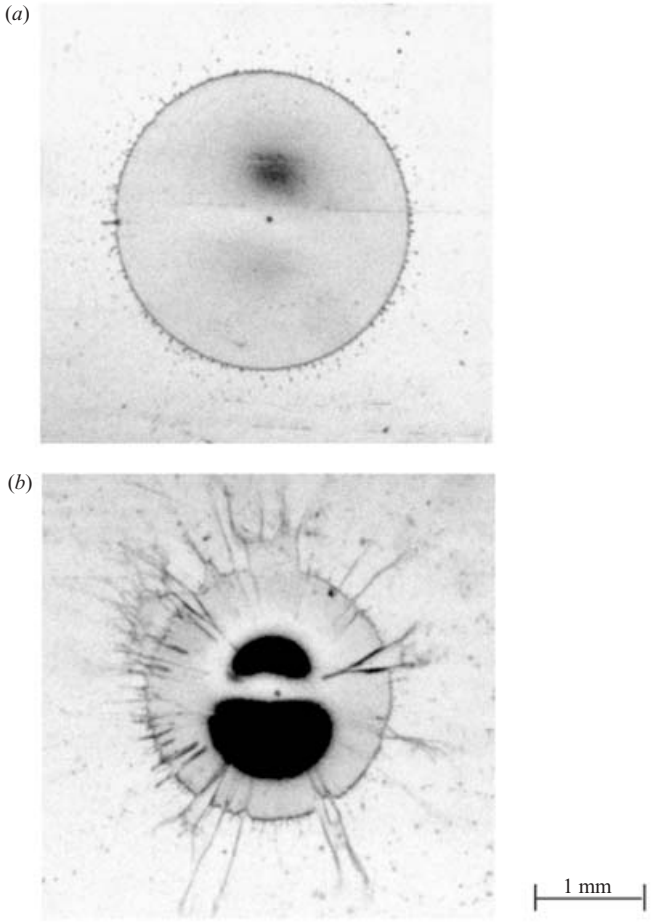

FIGURE 8. (*a*) Early splashing ($D_d = 0.55$ mm, $V_d = 30\,\mathrm{m\,s^{-1}}$, $R_a = 0.03\,\mu$m). (*b*) Detachment of the fluid sheets from top of the spreading film ($D_d = 0.55$ mm, $V_d = 40\,\mathrm{m\,s^{-1}}$, $R_a = 0.03\,\mu$m).

spreading. The viscous work (W) was estimated using a simple expression,

$$W = \int_0^{t_c^*} \int_{\Omega} \Phi \,\mathrm{d}\Omega \,\mathrm{d}t \approx \Phi\, \Omega\, t_c^*, \tag{3.1}$$

where Ω is the volume of viscous fluid, t_c^* the time taken for the droplet to spread, and Φ the viscous dissipation function. Pasandideh-Fard *et al.* (1996) estimated Φ to be:

$$\Phi = \mu \left(\frac{V_d}{\delta} \right)^2, \tag{3.2}$$

where μ is the liquid viscosity and δ the viscous boundary-layer thickness for axisymmetric stagnation-point flow. A simple model of droplet spreading was used to calculate

$$t_c^* = \frac{8 D_d}{3 V_d}. \tag{3.3}$$

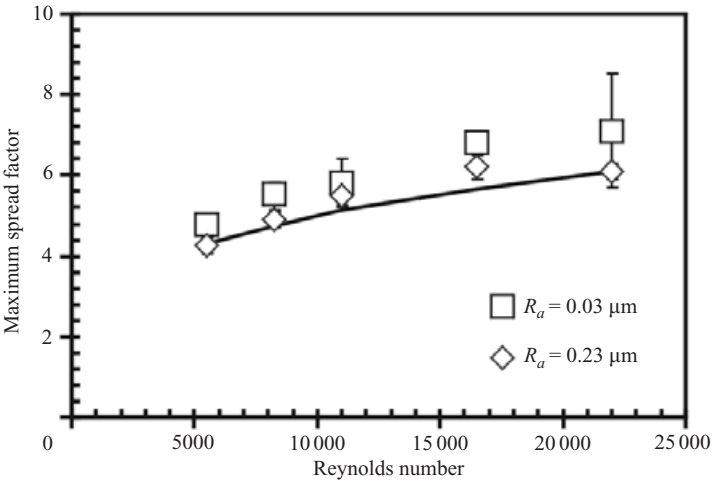

FIGURE 9. Maximum spread factor versus the Reynolds number for a 0.55 mm water droplet on two surfaces with different roughnesses, □, $R_a = 0.03\,\mu m$; ◇, 0.23 μm compared to —, the theoretical value from (3.4).

Neglecting surface energy, a reasonable assumption if $We \gg Re^{1/2}$, Pasandideh-Fard *et al.* (1996) predicted the maximum spread factor varies as

$$\xi_{max} = 0.5\ Re^{1/4}. \tag{3.4}$$

Equation (3.4) is shown in figure 9. Given the simplicity of the model, agreement between the predictions and experimental measurements was reasonable, the difference being at most 15% of the measured spread factor on the smoother surface ($R_a = 0.03\,\mu m$). The calculated values were much closer to the measurements on the rougher surface ($R_a = 0.23\,\mu m$), but this agreement may be fortuitous, since the model did not account for variation in surface roughness.

3.3. *Number of fingers*

Rayleigh (1900) and Taylor (1950) did a linear instability analysis of the interface between two fluids of different density, and showed that it is unstable (the so-called Rayleigh–Taylor instability) when accelerated towards the heavier fluid. Surface tension stabilizes the interface (Chandrasekhar 1961), and produces a mode of maximum instability at which the amplitude of perturbations grows fastest. More recently, Chen, Schrock & Peterson (1997) analysed the motion of a cylindrical surface expanding radially, and showed that the Rayleigh–Taylor instability depends not only on the acceleration, but also the velocity of the interface.

When a drop collides with a solid surface, the edge of the radially expanding liquid sheet formed is subjected to a large deceleration, triggering Rayleigh–Taylor instability. Kim *et al.* (2000) analysed this instability using potential flow equations in a cylindrical coordinate system. They neglected fluid viscosity, whose effect they argued would be small immediately after impact when the fluid is mainly driven by inertial forces. The equations were solved numerically to give the fastest growing wavelength. In this paper, we use the model of Kim *et al.* (2000), except that we solve the equations analytically, rather than numerically as they did.

In the discussion below the mathematical model is described only briefly; further details of equations are given by Kim *et al.* (2000). To make comparison easier, we

have used the same symbols as they did: the flow parameters are non-dimensionalized using droplet radius (R_d) as a characteristic length and impact velocity (V_d) as a characteristic velocity. However, it is conventional in experimental studies to define the Weber number using the droplet diameter (D_d) as a length scale so that $We = \rho V_d^2 D_d/\sigma$. To be consistent with previously published data we have used this definition, whereas Kim *et al.* (2000) defined their Weber number based on droplet radius (R_d). For this reason their Weber number values are half those of ours for the same impact conditions.

The velocity potential (ϕ) is defined to satisfy the following equations:

$$v_r = \frac{\partial \phi}{\partial r}, \tag{3.5}$$

$$v_\theta = \frac{1}{r}\frac{\partial \phi}{\partial \theta}, \tag{3.6}$$

where r is the radial distance from the droplet centre and θ is the azimuthal angle. Small disturbances of the velocity potential ϕ and outer droplet radius R can be described by writing:

$$\phi = \phi_0(t, r) + \phi_1(t, r, \theta), \tag{3.7}$$

$$R = R_0(t) + R_1(t, \theta), \tag{3.8}$$

where ϕ_0 and R_0 are unperturbed values and ϕ_1 and R_1 are small perturbations. For potential flow, ϕ satisfies the Laplace equation

$$\nabla^2 \phi = 0. \tag{3.9}$$

The axisymmetric flow of the droplet away from the centre is modelled as a line mass source with strength M:

$$\phi_0 = M(t) \ln r. \tag{3.10}$$

Using (3.5) and (3.6), the boundary condition at the edge of the expanding sheet ($r = R_0 + R_1$) is

$$\frac{\partial \phi_0}{\partial r} + \frac{\partial \phi_1}{\partial r} = \frac{\partial R_0}{\partial t} + \frac{\partial R_1}{\partial t} + \frac{1}{r^2}\frac{\partial \phi_1}{\partial \theta}\frac{\partial R_1}{\partial \theta}. \tag{3.11}$$

The boundary condition at the free surface of the liquid at $r = R_0 + R_1$ is

$$\frac{\partial \phi}{\partial t} + \tfrac{1}{2}|\nabla \phi|^2 + \frac{2\kappa}{We} = \Delta P_0. \tag{3.12}$$

ΔP_0 is the pressure difference across the interface and κ the interface curvature which can be approximated as:

$$\kappa \approx \frac{1}{R_0} - \frac{1}{R_0^2}\left(R_1 + \frac{\partial^2 R_1}{\partial \theta^2}\right). \tag{3.13}$$

Arbitrary perturbations ϕ_1 and R_1 can be applied by superposition of normal modes consisting only of sinusoidal terms:

$$\phi_1 = \sum_{m=1}^{\infty} A_m(t) r^m \cos m\theta, \tag{3.14}$$

$$R_1 = \sum_{m=1}^{\infty} f_m(t) \cos m\theta. \tag{3.15}$$

Combining (3.11)–(3.15) gives (see Kim *et al.* 2000 for details)

$$mA_m R_0^{m-1} = \dot{f}_m + \frac{M}{R_0^2} f_m, \tag{3.16}$$

$$f_m \left[\frac{\dot{M}}{R_0} - \frac{M^2}{R_0^3} + \frac{2(m^2-1)}{We} \frac{1}{R_0} \right] + R_0^m \dot{A}_m + mMR_0^{m-2} A_m = 0. \tag{3.17}$$

Equations (3.16) and (3.17) give an equation for the shape perturbation amplitude f_m:

$$\ddot{f}_m + a(t)\dot{f}_m + b(t) f_m = 0, \tag{3.18}$$

where the variable coefficients $a(t)$ and $b(t)$ are

$$a(t) = 2\frac{\dot{R}_0}{R_0}, \tag{3.19}$$

$$b(t) = \frac{(m+1)}{R_0^3} \left[\frac{2m(m-1)}{We} + R_0^2 \ddot{R}_0 \right]. \tag{3.20}$$

Evaluation of the coefficients $a(t)$ and $b(t)$ requires an expression for the spreading rate of the droplet, $R_0(t)$. Pasandideh-Fard *et al.* (1996) developed a simple model to estimate the rate at which the radius expands. They predicted that the evolution of droplet diameter can be expressed as:

$$\frac{D_0}{D_{max}} = \sqrt{\frac{3}{8} \frac{V_d}{D_d} t^*}. \tag{3.21}$$

From (3.4), substituting $D_d = 2R_d$, we obtain:

$$D_{max} = R_d Re^{1/4}. \tag{3.22}$$

Combining (3.21) and (3.22), and substituting $D_0 = 2R_0$ yields

$$R_0 = \frac{\sqrt{3}}{8} Re^{1/4} \sqrt{t}. \tag{3.23}$$

For the range of Re in our experiments ($2 \times 10^3 < Re < 5 \times 10^4$), the value of the coefficient $A = (\sqrt{3}/8)Re^{1/4}$ varies from 1.4 to 3.2. Kim *et al.* (2000) demonstrated that varying A over this range has little effect on the results from the model and assumed $A = 2$, a reasonable mean value that agrees with available experimental data for droplet spreading rates.

By choosing $R_0 = 2\sqrt{t}$, equations (3.19) and (3.20) can be rewritten as

$$a(t) = \frac{1}{t}, \tag{3.24}$$

$$b(t) = \frac{m(m^2-1)}{4We} \frac{1}{t^{3/2}} - \frac{m+1}{4} \frac{1}{t^2}. \tag{3.25}$$

Substituting (3.24) and (3.25) into (3.18), and defining $t = z^4$ yields

$$z^2 \frac{\mathrm{d}^2 f_m}{\mathrm{d}z^2} + z \frac{\mathrm{d}f_m}{\mathrm{d}z} + 16(\alpha z^2 - \beta) f_m = 0, \tag{3.26}$$

where $\alpha = m(m^2-1)/4We$ and $\beta = m + 1/4$. Equation (3.26) is Bessel's equation and has an analytical solution (McLachlan 1934)

$$f_m(t) = c_1 J_{4\sqrt{\beta}}\left(4\sqrt{\alpha} t^{1/4}\right) + c_2 Y_{4\sqrt{\beta}}\left(4\sqrt{\alpha} t^{1/4}\right), \tag{3.27}$$

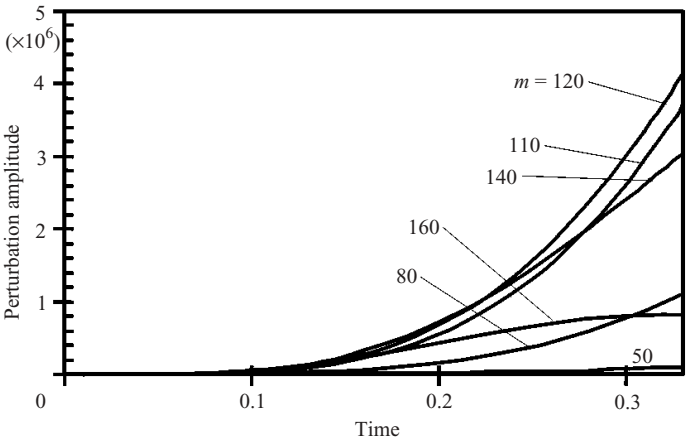

FIGURE 10. Perturbation amplitude of various wavenumbers until $t = 1/3$. Initial conditions at $t = t_i$ are $f_m = 1$ and $\dot{f}_m = 0$. The computation was performed for $t_i = 0.01$ and $We = 12\,055$ corresponding to an impact velocity of $40\,\mathrm{m\,s^{-1}}$.

where $J_{4\sqrt{\beta}}$ and $Y_{4\sqrt{\beta}}$ are Bessel functions of the first and second kind, of order $4\sqrt{\beta}$, respectively. The constants c_1 and c_2 have to be determined from initial conditions, assumed to be $f_m(0) = 1$ and $\dot{f}_m(0) = 0$. For $\beta > 0$, $J_{4\sqrt{\beta}}(0) = 0$ and $Y_{4\sqrt{\beta}}(0) = -\infty$. To obtain a finite initial perturbation ($f_m(0) = 1$), we set $c_2 = 0$.

Evaluating c_1 is complicated by the fact that a mathematical singularity occurs as $t \to 0$, when both the velocity and deceleration of the spreading liquid sheet reach infinity. In reality, the droplet is slightly flattened as it approaches the surface owing to increased air pressure between the liquid and solid surfaces (Thoroddsen & Sakakibara 1998; Mehdi-Nejad, Mostaghimi & Chandra 2003) so that the liquid sheet starts from a finite initial radius. To account for this in the model, the initial conditions were applied at a finite time (t_i) rather than at $t = 0$, so that $f_m(t_i) = 1$. Then, (3.27) can be expressed as

$$f_m(t) = \frac{J_{4\sqrt{\beta}}\left(4\sqrt{\alpha}t^{1/4}\right)}{J_{4\sqrt{\beta}}\left(4\sqrt{\alpha}t_i^{1/4}\right)}. \tag{3.28}$$

Kim *et al.* (2000) chose $t_i = 0.01$ and showed that varying this number had little effect on their calculations; we therefore used the same value. The choices of t_i and $f_m(t_i)$ are arbitrary and altering their values would not change our results. If we selected a larger perturbation, or an earlier time to apply the initial condition, all calculated perturbation amplitudes would increase proportionately. However, the absolute values of perturbation amplitude have no physical significance – we are only interested in relative magnitudes to determine the wavenumber of the disturbance that grows fastest. We evaluated values of the perturbation amplitude f_m from (3.28). To check our results, we also solved (3.18) numerically using a fourth-order Runge–Kutta method and confirmed that the analytical solution matched the numerical results.

Figure 10 shows the magnitude of the perturbation amplitude as a function of time for different wavenumbers and $We = 12\,055$ (corresponding to $D_d = 0.55\,\mathrm{mm}$ and $V_d = 40\,\mathrm{m\,s^{-1}}$). Perturbations with a wavenumber $m = 120$ grew fastest; those with greater and smaller values of m grew at a slower rate, and eventually decayed. The wavenumber of the fastest growing perturbation remained relatively constant as the droplet spread. Figure 11 shows the variation of the wavenumber of maximum

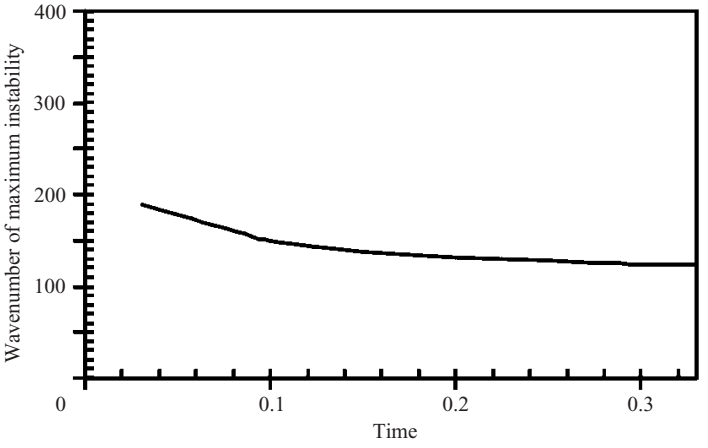

FIGURE 11. Wavenumber of maximum instability versus time at early stages of spreading. Initial conditions at $t = t_i$ are $f_m = 1$ and $\dot{f}_m = 0$. The computation was performed for $t_i = 0.01$ and $We = 12\,055$ corresponding to an impact velocity of $40\,\mathrm{m\,s^{-1}}$.

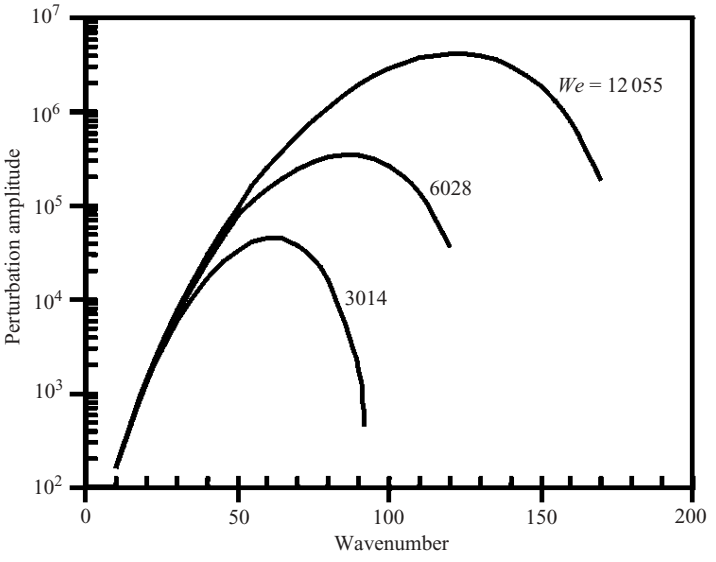

FIGURE 12. Perturbation amplitude versus wavenumbers for different values of Weber number. Initial conditions at $t = t_i$ are $f_m = 1$ and $\dot{f}_m = 0$. The computation was performed for $t_i = 0.01$.

instability with time: after a small initial decrease, the wavenumber did not change further. For comparison with experimental results, we used wavenumbers calculated at $t = 0.33$, when their value was constant. This corresponds to a time when the liquid sheet is spreading, after which the number of fingers would be constant.

Figure 12 shows calculated values of the perturbation amplitude at $t = 0.33$ as a function of wavenumber for different values of Weber number. It can be seen that as *We* increases the peak of the amplitude curve shifts to higher wavenumbers. Since the wavenumber that produces the maximum perturbation amplitude corresponds to the number of fingers (N) formed around the droplet periphery, this prediction agrees with the experimental observation that N increases with *We* (see table 1).

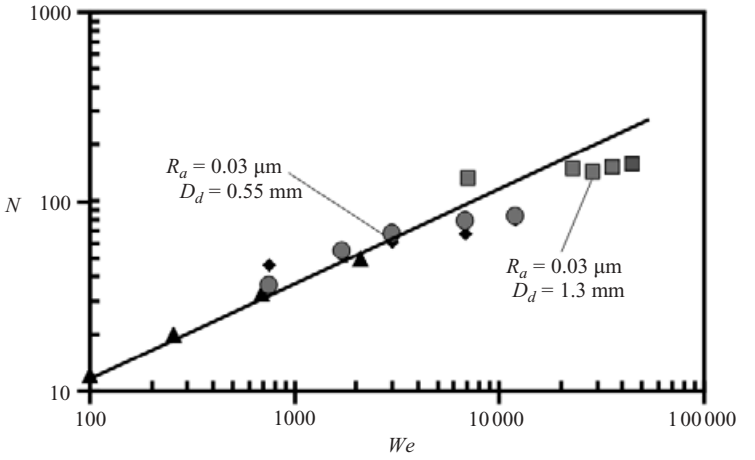

FIGURE 13. The number of fingers versus Weber number. The solid line corresponds to the most unstable wavenumber. ▲, Marmanis & Thoroddsen (1996); ◆, $R_a = 0.23\,\mu m$; —, theory.

We calculated the wavenumbers corresponding to the fastest growing perturbation for $10^2 < We < 10^5$; the solid line in figure 13 shows predicted values. On the same figure, we plotted the number of fingers around impacting droplets in our experiments. Data at lower Weber numbers were obtained from the results of Marmanis & Thoroddsen (1996), who counted the fingers around inkblots formed by letting drops fall onto a sheet of paper. Each of our data points represents the average of 10 measurements. The variation in N was at most $\pm 10\%$, which was smaller than the size of symbols used in figure 13.

The numbers of fingers observed in experiments agree reasonably well with predictions from the mathematical model over the entire range of data, $10^2 < We < 5 \times 10^4$, supporting the hypothesis that fingering around splashing droplets is caused by Rayleigh–Taylor instability. For 0.55 mm diameter droplets, N increases with We, but appears to reach a maximum for $We \sim 10^4$, where data points in figure 13 fall below predicted values. We speculate that for a given droplet diameter there may be an upper limit to the number of fingers that can form: capillary forces would oppose too small a radius at the tips of fingers, restricting their number. When droplet diameter was increased to 1.3 mm, the number of fingers increased, but soon reached a plateau.

A curve fit through the solid line in figure 13 showed that an equation of the form:

$$N = 1.14\, We^{1/2} \tag{3.29}$$

agrees with the calculated values of the fastest growing wavenumber within $\pm 3\%$, and can be used to estimate the number of fingers around an impacting drop.

The model does not account for the effect of surface roughness, since it assumes that fingers are initiated at the instant a droplet first contacts the surface and do not merge with each other while spreading. However, our experiments show that the number of fingers is slightly less on a rough surface than it is on a smooth surface (see figure 13 and table 1), confirming the earlier findings of Range & Feuillebois (1998). Photographs of splashing drops of water (Thoroddsen & Sakakibara 1998) and molten tin (Aziz & Chandra 2000) show that the number of fingers decreases a little during spreading. Close examination of the edges of spreading droplets by Thoroddsen & Sakakibara (1998) confirms that some fingers merge during droplet spreading, so that the number counted at the maximum extension of the drop is

a little less than those initiated at impact. It is possible that increasing surface roughness promotes this merging of fingers by retarding their radial motion, reducing the number of fingers visible around a droplet by the time it has fully spread.

4. Summary and conclusions

We designed and built an experimental apparatus to observe high-speed impact of a water droplet on a stainless steel surface under controlled conditions. The principal parameters varied were droplet diameter (0.55 or 1.3 mm), impact velocity (10–50 m s^{-1}) and surface roughness (0.03 or 0.23 μm). We photographed the deformation of impinging droplets and measured the number of fingers and maximum diameter of droplet after spreading. Droplets spread into a thin liquid film after impact. The maximum diameter to which droplets spread was predicted with reasonable accuracy by an energy conservation model of droplet impact.

Periodic instabilities were observed around the edges of spreading droplets. As impact velocity increased, the amplitude of these instabilities increased and they formed finger-shaped protrusions. The size and number of fingers increased with impact velocity, eventually growing so long that their tips broke off, forming satellite droplets. Increasing surface roughness reduced the number of fingers, but increased their size. At high impact velocities (above 40 m s^{-1}) the liquid film ruptured in several places.

A mathematical model was used to predict the number of fingers. The model calculated the wavenumber of the fastest growing perturbation, assuming that a Rayleigh–Taylor instability developed at the decelerating liquid–air interface. Predictions from the model agreed reasonably well with the number of fingers around impacting droplets over the entire range of available experimental data, $10^2 < We < 5 \times 10^4$.

The authors would like to express their appreciation to the Natural Sciences and Engineering Research Council of Canada (NSERC), Material and Manufacturing Ontario (MMO), and the Thermal Spray Consortium at the University of Toronto for their support.

REFERENCES

Allen, R. F. 1975 The role of surface tension in splashing. *J. Colloid Interface Sci.* **51**, 350–351.

Aziz, S. D. & Chandra, S. 2000 Impact, recoil and splashing of molten metal droplets. *Intl J. Heat Mass Transfer* **43**, 2841–2857.

Bhola, R. & Chandra, S. 1999 Parameters controlling solidification of molten wax droplets falling on a solid surface. *J. Mater. Sci.* **34**, 4883–4894.

Bussmann, M., Aziz, S. D., Chandra, S. & Mostaghimi, J. 1998 3-D Modelling of thermal spray droplet splashing. *Proc. 15th Intl Thermal Spray Conf. ASM International, Materials Park, OH*, pp. 413–418.

Bussmann, M., Chandra, S. & Mostaghimi, J. 2000 Modelling the splash of a droplet impacting a solid surface. *Phys. Fluids* **12**, 3121–3132.

Chandra, S. & Avedisian, C. T. 1991 On the collision of a droplet with a solid surface. *Proc. R. Soc. Lond.* A **432**, 13–41.

Chandrasekhar, S. 1961 *Hydrodynamic and Hydromagnetic Stability*, Chap. 10. Oxford University Press.

Chen, X. M., Schrock, V. E. & Peterson, P. F. 1997 Rayleigh–Taylor instability of cylindrical jets with radial motion. *Nucl. Engng Design* **177**, 121–129.

Cossali, G. E., Coghe, A. & Marengo, M. 1997 The impact of a single drop on a wetted solid surface. *Exps. Fluids* **22**, 463–472.

Kim, H. Y., Feng, Z. C. & Chun, J. H. 2000 Instability of a liquid jet emerging from a droplet upon collision with a solid surface. *Phys. Fluids* **12**, 531–541.

Loehr, K. F. 1990 Étalement et éclatement de gouttes. PhD Thesis, Université Pierre et Marie Curie, Paris, France.

Loehr, K. F. & Lasek, A. 1990 Splashing of drops. *Arch. Mech.* **42**, 507–513.

McLachlan, N. W. 1934 *Bessel Functions for Engineers*, pp. 1–15. Oxford University Press.

Mao, T. 1996 Impact of liquid droplets on solid surfaces and its application to carryover deposition in kraft recovery boilers. PhD thesis, University of Toronto, Ontario, Canada.

Marmanis, H. & Thoroddsen, S. T. 1996 Scaling of the fingering pattern of an impacting drop. *Phys. Fluids* **8**, 1344–1346.

Mehdi-Nejad, V., Mostaghimi, J. & Chandra, S. 2003 Air bubble entrapment under an impacting droplet. *Phys. Fluids* **15**, 173–183 .

Mundo, C., Sommerfeld, M. & Tropea, C. 1995 Droplet–wall collisions: experimental studies of the deformation and break up process. *Intl J. Multiphase Flow* **21**, 151–173.

Pasandideh-Fard, M., Qiao, Y. M., Chandra, S. & Mostaghimi, J. 1996 Capillary effects during droplet impact on a solid surface. *Phys. Fluids* **8**, 650–659.

Range, K. & Feuillebois, F. 1998 Influence of surface roughness on liquid drop impact. *J. Colloid Interface Sci.* **203**, 16–30.

Rayleigh, Lord 1900 Investigation of the character of the equilibrium of an incompressible heavy fluid of variable density. *Sci. Papers* vol. 2, p. 200. Cambridge University Press.

Rein, M. 1993 Phenomena of liquid drop impact on solid and liquid surfaces. *Fluid Dyn. Res.* **12**, 61–93.

Rein, M. 1995 Wave phenomena during droplet impact. *IUTAM Symp. on Waves in Liquid/Gas and Liquid/Vapour Two-Phase Systems*, pp. 171–190. Kluwer.

Sharp, D. H. 1984 An overview of Rayleigh–Taylor instability, *Physica* **12**D, 3–18.

Stow, C. D. & Hadfield, M. G. 1981 An experimental investigation of fluid flow resulting from the impact of water drop with an unyielding surface. *Proc. R. Soc. Lond.* A **373**, 419–441.

Taylor, G. I. 1950 The instability of liquid surfaces when accelerated in a direction perpendicular to their plane. *Proc. R. Soc. Lond.* A **201**, 193–196.

Thoroddsen, S. T. & Sakakibara, J. 1998 Evolution of the fingering pattern of an impacting drop. *Phys. Fluids* **10**, 1359–1374.

Worthington, A. M. 1876 On the forms assumed by drops of liquids falling vertically on a horizontal plate. *Proc. R. Soc. Lond.* **25**, 261–271.

Worthington, A. M. 1907 *The Splash of a Drop*. Society for Promoting Christian Knowledge, London, UK.

Yang, J. C., Chien, W., King, M. D. & Grosshandler, W. L. 1997 A simple piezoelectric droplet generator. *Exps. Fluids* **23**, 445–447.

Yarin, A. L. & Weiss, D. A. 1995 Impact of drops on solid surfaces: self-similar capillary waves, and splashing as a new type of kinematic discontinuity. *J. Fluid Mech.* **283**, 141–173.